Non-Equilibrium Numerical Study of a Two-Stage Microwave Electrothermal Thruster

V. P. Chiravalle * R. B. Miles † and E. Y. Choueiri ‡
Princeton University
Princeton, NJ, 08544
Phone: (609) 258-5213
E-mail: chiravle@princeton.edu

IEPC–01–194

A new two-stage microwave electrothermal thruster concept, that incorporates a supersonic energy addition section, is explored numerically by using a sophisticated two-temperature, non-equilibrium model. This model includes the complete system of both the Maxwell equations and the Navier-Stokes equations for the case of a helium flow with different electron and heavy species temperatures and with finite rate ionization kinetics. Results from a simulation of the supersonic stage of the thruster are presented, involving a 200 mg/sec helium flow where it is assumed that 5.5 kW is absorbed in subsonic stage and an additional 5 kW is absorbed in the supersonic stage. It is shown that both the specific impulse and thrust increase by 16 %, compared with the case without supersonic energy addition.

Introduction

A microwave electrothermal thruster is a space propulsion system that uses a microwave plasma to heat a low molecular weight propellant gas to a high temperature, and like in a conventional rocket engine the propellant gas then expands isentropically in a nozzle to produce thrust. Unlike other electrothermal propulsion systems, such as resistojets and arcjets,[1] microwave thrusters have not been used on spacecraft. A state-of-the-art, 2 kW hydrazine arcjet has demonstrated a specific impulse of roughly 600 sec and an efficiency of 30 % during a 550-h test.[2] The fact that a microwave-sustained plasma can be created without electrodes and can be maintained away from the material surfaces of the thruster, may allow for large reductions in thruster erosion and significant improvements in overall lifetime, compared with arcjets. From a fundamental point of view, a microwave plasma can be sustained in a stable location in a subsonic flow only for a certain range of specific powers.[3] This behavior is analogous to the stability limit of a flame, and therefore the specific impulse of a microwave thruster, with heating only in the subsonic plenum, is limited. One possible way to circumvent this limitation and to realize higher performance in terms of specific impulse and thrust is to add additional energy to the propellant in the supersonic region of the flow, creating a supersonic "afterburner". This can be accomplished by using additional microwave energy to create another plasma in the supersonic region of flow.

Previous Work

Different configurations have been explored for coupling microwave power to a gas, the most promising for thruster applications is the cylindrical resonant cavity design, employing either the TM_{011} or TM_{012} microwave mode structure. The first thruster of this kind was built in the early 1980's and it consisted of a cylindrical microwave resonant cavity at 2.45 GHz and a quartz tube, arranged concentrically.[4] He or N_2 gas flowed

*Graduate Student, Mechanical & Aerospace Engineering

†Professor, Mechanical & Aerospace Engineering

‡Chief Scientist at EPPDyL. Assistant Professor, Mechanical & Aerospace Engineering

Presented as Paper IEPC–01–128 at the 27th International Electric Propulsion Conference, Pasadena, CA, 15–19 October, 2001.

through the quartz tube, where the walls stabilized the microwave plasma on the centerline. The gas then exited through a quartz nozzle connected to the tube. It was shown that the ratio of power absorbed by the plasma to the incident power delivered to the cavity, the microwave coupling efficiency, could be made to exceed 95% with proper tuning of the cavity for discharges sustained at pressures from 40 to 1000 Torr.[4] Excessive heating and erosion of the quartz nozzle limited the input power to less than 2 kW for mass flow rates in the range of 100 mg/sec. Another prototype thruster utilizing a cylindrical resonant cavity at 2.45 Ghz with a free-floating plasma inside the cavity has operated successfully at power levels of up to 2.2 kW and pressures as high as 3 atm with He, N_2, NH_3 and H_2 as propellants.[5] In that design the plasma is stabilized by flow swirl created from tangential gas injection into the cavity. The gas exits the cavity through a graphite nozzle. Spectroscopic measurements were made of free-floating He plasmas in the cavity, stabilized by a bluff body, and the results indicate that the electron temperature of these discharges is roughly constant at 12,000 K over a range of incident powers from 0.5 to 1.0 kW and a range of pressures from 1.0 to 3.0 atm.[6]

In addition to these experimental efforts, numerical work has been done to model the physical processes occurring in microwave-sustained discharges. The size, shape, location and peak temperature of the free-floating He discharges, stabilized by a bluff body, discussed above have been reasonably well predicted by a computational model consisting of a low Mach number formulation of the Navier-Stokes and the Maxwell equations.[7] Thermodynamic equilibrium was assumed, in the sense that both electrons and heavy species have the same temperature and that the electron concentration is determined from the Saha relation. Subsequently, the model was extended to include a converging nozzle section so that realistic thruster configurations could be simulated, and a parametric study of the effect of nozzle throat area, discharge pressure and absorbed power on the location of the plasma in a resonant cavity thruster was performed.[8] For simulations at a microwave frequency of 0.915 GHz, a helium mass flow rate of 1.9 g/sec (1 atm plenum pressure) and an incident power of 40 KW, a toroidal plasma was observed off the cavity centerline. As the cavity length was changed, detuning the cavity from resonance and reducing the power absorbed by the plasma, it was shown that the plasma would move back on the centerline. A similar single-temperature, equilibrium model was used to show that a stable plasma could be created in a supersonic argon flow, using microwaves at 2.45 GHz.[9] In this work the plasma forms a toroidal shape, with most of the energy addition occurring in the boundary layer at the walls of the diverging nozzle. In the region of maximum heating the assumption of equal electron and heavy species temperatures was shown to be inaccurate and would predict an electron density which was too low, by at least an order of magnitude.[9] Numerical models including the effects of distinct electron and heavy species temperatures have been developed and used to simulate arcjets[10,11] and MPD thrusters,[12,13] however until now such a two-temperature model has not been used to study a microwave thruster.

The goal of the present work is to simulate the supersonic energy addition section of such a two-stage microwave thruster, with helium as the propellant, using a computational model which includes the effects of separate electron and heavy species temperatures and a finite ionization rate.

Outline

The physical model and the numerical techniques used in the present study are described briefly in the next section. The results from a computation of the supersonic energy addition section of the two-stage microwave thruster are presented following the description of the physical model. These results are compared with previous work and an outline of necessary future work is given in the conclusions section.

Physical Model

The physical model used in this work shares many common features with a previous model, developed by the authors to study supersonic argon plasmas.[9] The microwave field in the cylindrical waveguide, which forms the supersonic energy addition stage of the thruster is solved, using essentially the same finite element code as in the previous work.[9] This code finds the axial and radial components of the complex electric field, with each field component described by the Helmholtz

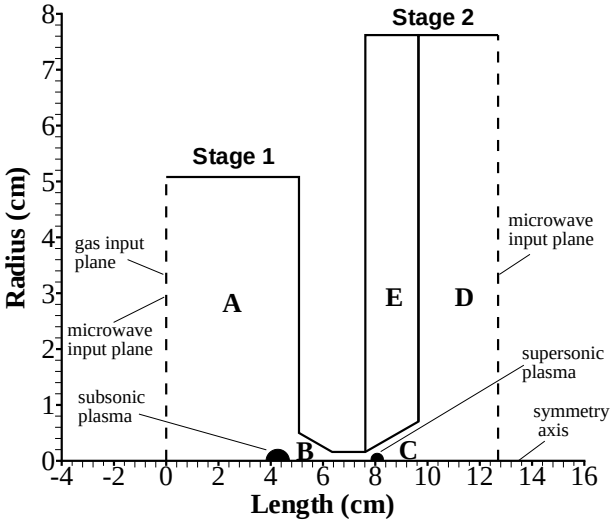

Fig. 1 The geometry used to simulate a two-stage microwave thruster. The subsonic plenum is labeled as A, the converging nozzle as B, the diverging nozzle as C, the transmission section of waveguide as D and the dielectric wall as E.

equation. The fluid model incorporates the same Navier-Stokes solver as well, with two additional equations, one for the electron density and another for the electron thermal energy. There are three types of particles in the model, electrons, ions and atoms. It is assumed that the heavy particles, atoms and ions, have the same temperature. Multi-level ionization is neglected, and it is further assumed that the number densities of electrons and ions are equal.

Flowfield Configuration

Since the main goal in this work is to study the supersonic energy addition concept, and not to evaluate the merits of various propellants, helium was chosen as the propellant for simplicity. A practical electrothermal thruster would use a storable space propellant such as hydrazine, ammonia or water. The geometry of the two-stage microwave thruster considered in this paper is illustrated in Fig. 1. The thruster consists of two cylindrical waveguides sections, one waveguide which brings microwave energy for the subsonic plasma, labeled Stage 1 in Fig. 1, and another which brings microwave energy for the supersonic plasma, labeled Stage 2. Stage 1 has a radius of 5.08 cm and Stage 2 has a radius of 7.63 cm. These values, and all the other dimensions to follow, were chosen to match closely a prototype two-stage thruster which is currently being built. In this ideal representation, microwave energy enters each of the waveguides separately, through one of the planes indicated by a dashed line in Fig. 1, and both of the waveguides are terminated by a perfectly conducting plate. Only supersonic energy addition is considered in this study. The complex electric field is specified at the microwave input plane of Stage 2, using a theoretical expression for a cylindrical, TM_{01} mode with the amplitude chosen so that the desired amount of power is absorbed by the supersonic plasma.

The propellant gas, helium, enters the plenum, section A, at $x = 0$ in Fig. 1, and is subsequently heated by a microwave-sustained plasma in Stage 1, which is not part of our simulation. The flow then moves through a converging conical nozzle, section B, which connects to a throat region with a radius of 1.59 mm. The supersonic energy addition section is labeled as section C and it is a diverging conical nozzle with a half angle of 15 degrees and a length of 2.03 cm. In this paper the fluid properties in section C are determined by solving the Navier-Stokes equations, with the throat conditions specified. We choose to study a case with 200 mg/sec flow rate and where 5.5 kW of microwave energy is added in the subsonic stage, representing one possible operating point for the prototype thruster. For such a flow the temperature at the throat would need to be 4000 K, and at this point we further assume an electron temperature of 8,000 K and an ionization fraction of 10^{-6}, in order to provide some initial electron density so that microwave heating can take place in the supersonic section. In Fig. 1 the diverging nozzle is labeled section E and consists of alumina ceramic, which has a dielectric constant of 9.0 and a loss tangent of 8×10^{-4}. The nozzle fills the entire cross section of the waveguide. The supersonic energy addition section of the real microwave thruster would have a radial antenna protruding into section E, which would act to couple microwave energy into sections C and E. The three-dimensional field pattern associated with this radial antenna is not considered in the present model, but rather it is assumed that microwaves propagate through the waveguide from the input plane into sections C and E, without interacting with the exhaust plume of the thruster in section D, and in this way the section

of waveguide between the input plane of Stage 2 and sections C and E acts like an antenna in the numerical simulation.

Navier-Stokes Equations

The unsteady axisymmetric Navier-Stokes equations, for a two-temperature monatomic gas with arbitrary degree of ionization, can be written in cylindrical coordinates in the following differential vector form[14]

$$\frac{\partial r\mathbf{U}}{\partial t} + \frac{\partial r\mathbf{F}(\mathbf{U})}{\partial x} + \frac{\partial r\mathbf{G}(\mathbf{U})}{\partial r} = \mathbf{S}, \qquad (1)$$

where x and r are the axial and radial directions, respectively. $\mathbf{U} = (\rho_e, \rho, u, v, E_h, E_e)^{\mathrm{T}}$ is the vector of conservation variables, with total mass density as ρ, electron mass density as ρ_e, axial velocity as u, and radial velocity as v. The total heavy particle energy density (thermal plus kinetic) is expressed as

$$E_h = \rho\left(\frac{3}{2}R_hT + 1/2[u^2+v^2]\right) + \beta\rho_e,$$

where R_h is the heavy particle gas constant, T is the heavy particle temperature, and $\beta\rho_e$ is the internal energy contribution due to ionization. The electron energy density is taken to be $E_e = (3/2)\rho_e R_e T_e$, where R_e is the electron gas constant and T_e is the electron temperature. The kinetic energy of the electrons has been neglected, as well as the contribution of the electron mass to the total mass density. The flux vectors, $\mathbf{F}(\mathbf{U}) = \mathbf{F^c}(\mathbf{U}) - \mathbf{F^d}(\mathbf{U})$ and $\mathbf{G}(\mathbf{U}) = \mathbf{G^c}(\mathbf{U}) - \mathbf{G^d}(\mathbf{U})$, are functions of the conservation variables and contain both convective and diffusive terms, represented by the superscripts c and d respectively. The convective flux vectors are[14]

$$\mathbf{F^c}(\mathbf{U}) = \begin{bmatrix} \rho_e u \\ \rho u \\ \rho u^2 + P \\ \rho uv \\ u(E_h + P_h) \\ u(E_e + P_e) \end{bmatrix},$$

$$\mathbf{G^c}(\mathbf{U}) = \begin{bmatrix} \rho_e v \\ \rho v \\ \rho uv \\ \rho v^2 + P \\ v(E_h + P_h) \\ v(E_e + P_e) \end{bmatrix},$$

while the diffusive flux vectors are

$$\mathbf{F^d}(\mathbf{U}) = \begin{bmatrix} 0 \\ 0 \\ \tau_{xx} \\ \tau_{xr} \\ -q_{hx} + u\tau_{xx} + v\tau_{xr} \\ -q_{ex} \end{bmatrix},$$

$$\mathbf{G^d}(\mathbf{U}) = \begin{bmatrix} 0 \\ 0 \\ \tau_{xr} \\ \tau_{rr} \\ -q_{hr} + u\tau_{xr} + v\tau_{rr} \\ -q_{er} \end{bmatrix}.$$

In the previous relations P is the total gas pressure. The heavy particle pressure is expressed as $P_h = \rho R_h T$ and the electron pressure is $P_e = \rho_e R_e T_e$. The viscous stresses are given by

$$\begin{aligned} \tau_{xx} &= \frac{4}{3}\mu\frac{\partial u}{\partial x} - \frac{2}{3}\mu\left(\frac{\partial v}{\partial r} + \frac{v}{r}\right), \\ \tau_{rr} &= \frac{4}{3}\mu\frac{\partial v}{\partial r} - \frac{2}{3}\mu\left(\frac{\partial u}{\partial x} + \frac{v}{r}\right), \\ \tau_{xr} &= \mu\left(\frac{\partial u}{\partial r} + \frac{\partial v}{\partial x}\right), \end{aligned}$$

with μ equal to the gas viscosity. The heat fluxes are

$$\begin{aligned} q_{hx} &= -k_h\frac{\partial T}{\partial x}, \\ q_{hr} &= -k_h\frac{\partial T}{\partial r}, \\ q_{ex} &= -k_e\frac{\partial T_e}{\partial x}, \\ q_{er} &= -k_e\frac{\partial T_e}{\partial r}, \end{aligned}$$

with k_h equal to the thermal conductivity of the heavy particles and k_e equal to the thermal conductivity of the electrons. The transport coefficients, μ, k_h and k_e, are discussed in the section on transport properties. The right hand side of Eqn. 1, $\mathbf{S}$, contains source terms that are due to the cylindrical symmetry of the problem, the finite ionization rate, the energy transfer between electrons and heavy particles, and the microwave

joule heating. The source term is given below

$$\mathbf{S} = \begin{bmatrix} rQ_{ion} \\ 0 \\ 0 \\ p + \frac{2}{3}\left(\tau_{xr} - \frac{2\mu v}{r}\right) \\ r(Q_e + Q_{in}) \\ r(-Q_e - Q_{in} + \langle \mathbf{i} \cdot \mathbf{E} \rangle) \end{bmatrix}.$$

In the above expression $\mathbf{i}$ is the current density vector and $\mathbf{E}$ is the electric field vector. The microwave joule heating term $\langle \mathbf{i} \cdot \mathbf{E} \rangle$ is described later, when the microwave field equations are discussed. The energy transfer from electrons to heavy particles due to elastic collisions is $Q_e = 3\rho_e \nu_{eH} k_b (T_e - T)/m_a$, where m_a is the mass of an atom, ν_{eH} is the electron collision frequency with heavy particles and k_b is the Boltzmann constant. The inelastic energy transfer term is $Q_{in} = \epsilon_e Q_{ion}/m_e$, where ϵ_e is the ionization potential. The ionization source term is calculated as $Q_{ion} = \rho_e S(N_a - N_e^2/Q_T)$, with the first term in this expression accounting for electron impact ionization and the second term three-body recombination. N_e is the electron number density and N_a is the atom number density. S is the ionization rate coefficient for helium,[3] and Q_T is the ratio of N_e^2/N_a at equilibrium, which is determined using the Saha equation. The ionization kinetics are controlled by the electron temperature in this model.

A conservative finite-volume numerical discretization, incorporating first-order scalar dissipation, is used to integrate the governing equations(1) in time until a steady state is reached, an approach that has been thoroughly validated by several authors.[14–16] The criteria for judging when a solution is properly converged is the reduction of the density residual by at least five orders of magnitude. Unlike the approach taken in previous work,[9] where time accuracy was achieved by marching the fluid equations with a single global time step, determined by the flow properties on the entire grid, in this work the time step is determined individually for each cell on the grid and the electron and heavy species equations are advanced with their own characteristic time step size. This last point is essential, because the addition of an electron energy equation adds stiffness to the problem. A simple grid was used for all the simulations in this work, consisting of 80 radial cells and 80 axial cells.

Transport Properties

In this work estimates of collision cross sections involving electrons and heavy particles are used to calculate the transport properties from first principles. The transport properties are defined in terms of energy-averaged mean free paths.[17] It is assumed that all particles have Maxwellian velocity distributions. The energy-averaged mean free paths of the particles in the model are given by

$$\begin{aligned} \lambda_e &= \frac{1}{2N_e Q_{ee} + \sqrt{2} N_e Q_{ei} + 2 N_a Q_{ea}}, \\ \lambda_i &= \frac{1}{\sqrt{2}(N_e Q_{ii} + N_a Q_{ia})}, \\ \lambda_a &= \frac{1}{\sqrt{2}(N_e Q_{ia} + N_a Q_{aa})}, \end{aligned}$$

where λ_e is the energy-average mean free path of an electron, λ_i is that of an ion and λ_a is that of an atom. In calculating the energy-averaged mean free paths of the atoms and ions, collisions with electrons are neglected, because $m_e/m_a << 1$. The energy-averaged collision cross section for electrons colliding with helium atoms is $Q_{ea} = 4 \times 10^{-20}$ m^2,[17] and for electrons colliding with ions it is $Q_{ei} = 5.85 \times 10^{-10} \log \Lambda / T_e^2$ m^2, where $\Lambda = 1.24 \times 10^7 \sqrt{T_e^3/N_e}$. It can be shown that $Q_{ei} = Q_{ee} = Q_{ii}$ for singly charged species. In this work the energy-averaged collision cross section for ions colliding with atoms is estimated as $Q_{ia} = Q_{ea}$. The corresponding atom-atom collision cross section, Q_{aa}, in units of m^2, is taken as

$$Q_{aa} = 4.14 \times 10^{-19} \left(1.147 \left[\frac{T}{5.67} \right]^{-0.145} + \left[\frac{T}{5.67} \right]^{-2} \right),$$

which was derived from a theoretical expression for the viscosity of helium atoms.[18] The average molecular speed of an electron is $C_e = \sqrt{8 R_e T_e/\pi}$ and of a heavy particle is $C_h = \sqrt{8 R_h T/\pi}$. Having defined these quantities, the viscosity and thermal conductivities can be written as

$$\begin{aligned} \mu &= m_a C_h \left(N_a \lambda_a + N_e \lambda_i \right), \\ k_h &= k_b \left(N_a C_h \lambda_a + N_e C_a \lambda_i \right), \\ k_e &= k_b N_e C_e \lambda_e. \end{aligned} \quad (2)$$

Next the quantities that are required to calculate the gas conductivity are presented. The total electron collision frequency with heavy particles, ν_{eH}, is given below as

$$\nu_{eH} = C_h \left(N_a Q_{ea} + N_e Q_{ei} \right).$$

The complex conductivity is responsible for the coupling between fluid and the microwave field. The complex conductivity is a function of N_e, ν_{eH}, and ω, the microwave angular frequency, according to the following expression

$$\sigma = \frac{N_e e^2}{m_e \left(\nu_{eH} + i\omega \right)}. \tag{3}$$

Maxwell Equations

For a TM_{01} mode in a cylindrical waveguide there are three components of the complex electromagnetic field, E_r, E_z, and H_θ. When calculating the electron joule heating term, only the electric field components are needed, as shown shortly. In cylindrical coordinates the Helmholtz equation that describes the axial component of the complex electric field, E_z, is[19]

$$\frac{1}{r}\frac{\partial}{\partial r} r \frac{\partial E_z}{\partial r} + \frac{\partial^2 E_z}{\partial x^2} + \beta^2 E_z = 0. \tag{4}$$

The corresponding equation for the radial component, E_r, is[19]

$$\frac{1}{r}\frac{\partial}{\partial r} r \frac{\partial E_r}{\partial r} + \frac{\partial^2 E_r}{\partial x^2} + \left(\beta^2 - \frac{1}{r^2} \right) E_r = 0. \tag{5}$$

In these equations the complex propagation constant, β, is such that $\beta^2 = \frac{\omega^2}{c^2}\left(1 - i\frac{\sigma}{\epsilon_0 \omega}\right)$, where c is the speed of light, ϵ_0 is the dielectric permittivity of free space and σ is the complex conductivity of the plasma, which was defined earlier. The finite element method is used to solve both Eqn. (5) and Eqn. (4) separately.[9] Using the computed values of the field components the microwave joule heating term is determined as given below

$$\langle \mathbf{i} \cdot \mathbf{E} \rangle = \frac{1}{4} \left(\sigma + \sigma^* \right) \left(E_r E_r^* + E_z E_z^* \right). \tag{6}$$

This completes the discussion of the equations that constitute the physical model.

Boundary Conditions

In this section the relevant boundary conditions for the equations above are reviewed, starting first with the microwave field components. E_r and E_z are specified at the inlet port, for each waveguide, Stage 1 and Stage 2, as discussed previously. Along the walls of each waveguide it is assumed that $E_z = 0$, and $\partial r E_r / \partial r = 0$. On each of the two terminating plates the following conditions hold true, $E_r = 0$ and $\partial E_z / \partial z = 0$. Finally on the centerline, the cylindrical symmetry of the problem implies that $E_r = 0$ and $\partial E_z / \partial r = 0$. This paper concentrates only on the microwave fields in Stage 2.

Because of the cell-centered scheme used by the Navier-Stokes solver it is necessary to specify the values of the flux vectors, $\mathbf{F}(\mathbf{U})$ and $\mathbf{G}(\mathbf{U})$, at the physical boundaries of the domain. Along the wall and centerline boundaries the convective fluxes are specified so that there are no mass, momentum or energy fluxes through these respective boundaries. In addition to the above specifications for the convective fluxes, the no slip conditions, $u = 0$ and $v = 0$, are applied at the wall boundary and the temperature of the wall is fixed at 500 K, this facilitates the computation of the diffusive fluxes, $\mathbf{F^d}(\mathbf{U})$ and $\mathbf{G^d}(\mathbf{U})$, at these locations. In addition the electrons are assumed to be adiabatic at the wall. The diffusive fluxes are zero at the gas inlet and exit planes. At the gas throat the fluid properties are prescribed, as mentioned before, and at the nozzle exit plane the convective fluxes are calculated by extrapolating the flow properties from the interior of the domain. Cylindrical symmetry is enforced along the centerline, by setting v and all partial derivatives with respect to r equal to zero.

Simulation Results

The results of a simulation involving 5 kW of supersonic energy addition are now presented, starting first with temperature and electron temperature contours. Fig. 2 shows the gas temperature contours in degrees Kelvin. The maximum temperature of 4700 K occurs at a point 0.8 mm downstream of the throat, where the electron temperature is 40,000 K. The electron temperature contours, are shown in Fig. 3. It is readily apparent that inside most of the nozzle, the electron temperature profile is markedly different than the

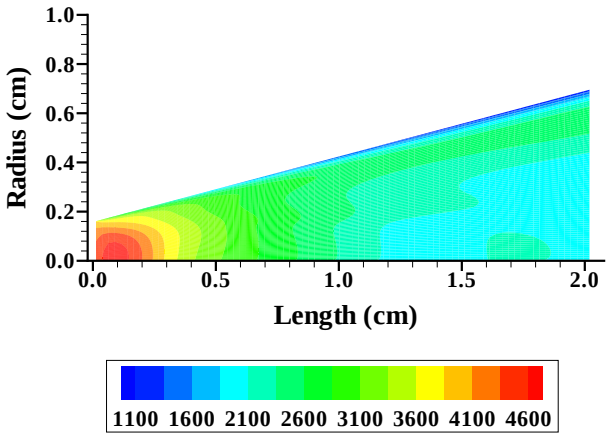

Fig. 2 Temperature contours inside the supersonic diverging nozzle section of the microwave thruster (in K).

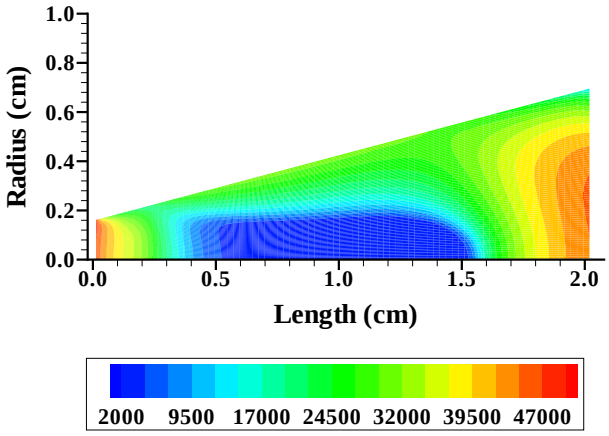

Fig. 3 Electron temperature contours inside the supersonic diverging nozzle section of the microwave thruster (in K).

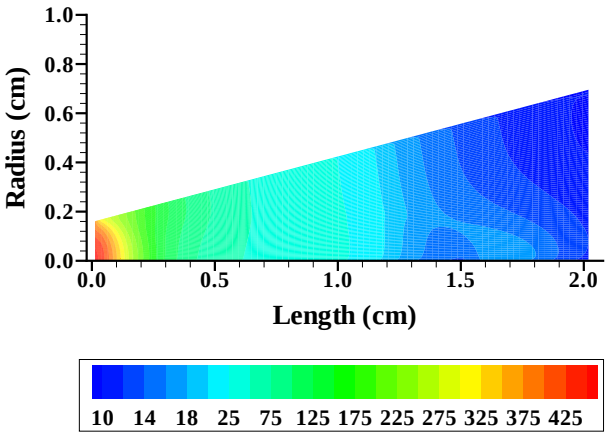

Fig. 4 Pressure contours inside the supersonic diverging nozzle section of the microwave thruster (in Torr).

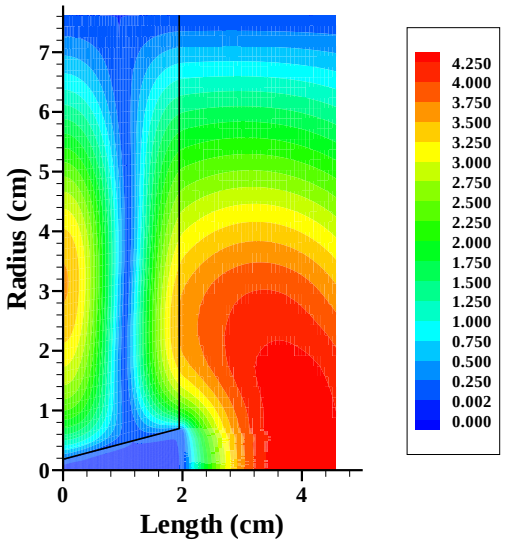

Fig. 5 Time-averaged value of the axial component of the complex electric field inside Stage 2 (in kV/cm). The solid black line indicates the boundary of the dielectric nozzle.

gas temperature profile, by an order of magnitude. The regions of maximum electron temperature correspond to the locations of maximum electric field strength, as one would expect. The disparity between the electron and heavy species temperature occurs, even though the gas pressure is several hundred Torr. The total pressure contours, in Torr, are shown in Fig. 4. The maximum pressure is roughly 460 Torr, just downstream of the throat.

The contours of the axial component of the electric field are shown in Fig. 5, where the solid black line indicates the boundary of the dielectric nozzle, section E in Fig. 1. The electric field is sharply attenuated, due to the presence of the plasma, from a value of 410 V/cm just above the dielectric nozzle boundary to a value of 2 V/cm just below. The corresponding radial component of the complex electric field is shown in Fig. 6. Unlike the axial component, the radial component of the field is not effected strongly by the presence of the plasma.

For microwaves at 2.45 GHz the critical electron

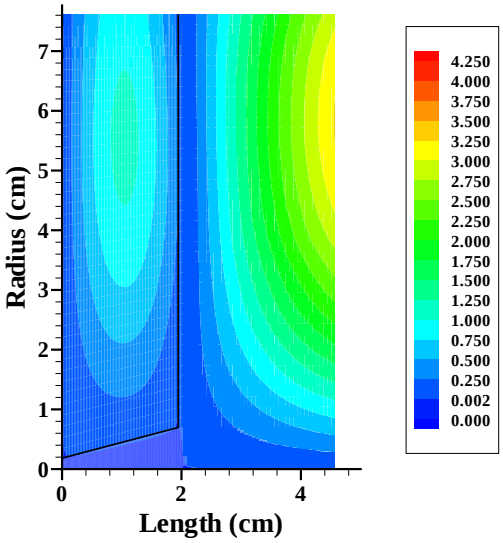

Fig. 6 Time-averaged value of the radial component of the complex electric field inside Stage 2 (in kV/cm). The solid black line indicates the boundary of the dielectric nozzle.

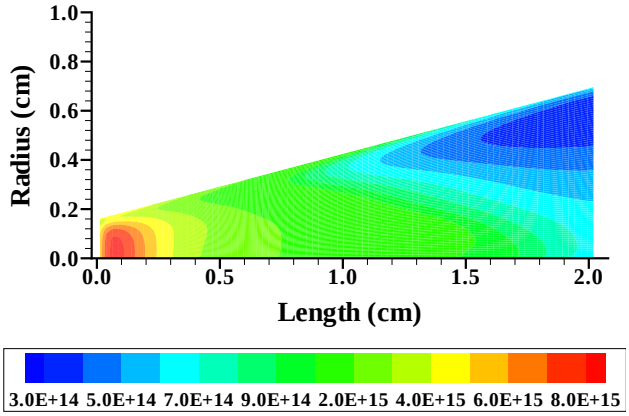

Fig. 7 Electron number density contours inside the supersonic diverging nozzle section (in $\mathbf{cm^{-3}}$).

number density is $7.45 \times 10^{10}\text{cm}^{-3}$. The electron number density in this problem is considerably larger than this, as shown in Fig. 7. The maximum electron number density is $8 \times 10^{15}\text{cm}^{-3}$, which occurs in the vicinity of the maximum temperature point, roughly 0.8 mm downstream of the throat. The electron number density drops to $3 \times 10^{13}\text{cm}^{-3}$ at the nozzle exit where the gas pressure is 10 Torr.

The Mach number contours inside the nozzle are shown in Fig. 8. The Mach number at the

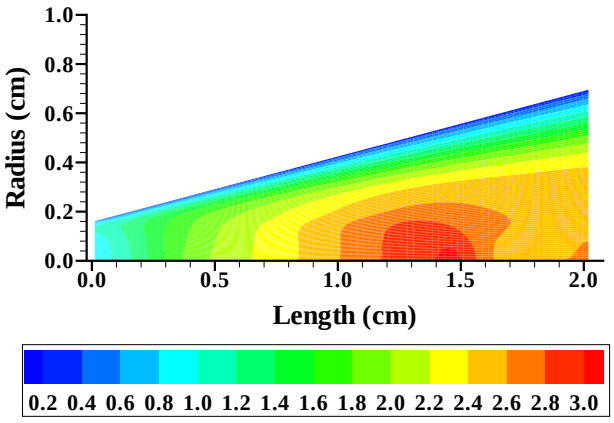

Fig. 8 Mach number contours inside the supersonic diverging nozzle section.

point 0.8 mm downstream of the throat, on the centerline is 1.02. The subsonic, laminar boundary layer is clearly visible. The Mach number increases to a maximum value of 3.0, 1.5 cm downstream of the throat and then decreases to a value of 2.6 at the nozzle exit. This Mach number decrease, and the increases in temperature and pressure that are associated with it, are due to energy transfer between electrons and heavy species which occurs in this region, on the order of 1 kW/cm^3, as indicated in Fig. 9. The energy transfer rate, $Q_e + Q_{in}$, is the sum of contributions from both elastic and inelastic processes. The heating rate of electrons by the microwave field, the joule heating rate, is shown in Fig. 10 for comparison. The joule heating rate just downstream of the throat is 440 kW/cm^3, and of this value, 315 kW/cm^3 is transferred to the heavy particles due to elastic and inelastic collisions. In the vicinity of the maximum temperature point, 0.8 mm downstream of the throat, the joule heating rate and the energy transfer rate are roughly the same, on the order of 200 kW/cm^3. Without supersonic energy addition the Mach number on the centerline, 0.8 mm downstream of the throat is 1.47, and the corresponding exit Mach number is 4.63. The axial velocity contours for the case of energy addition, are shown in Fig. 11. The axial velocity at the exit is 7.9 km/sec.

In order to see the effect of supersonic energy addition on the performance of the thruster, we ran an additional simulation of the supersonic

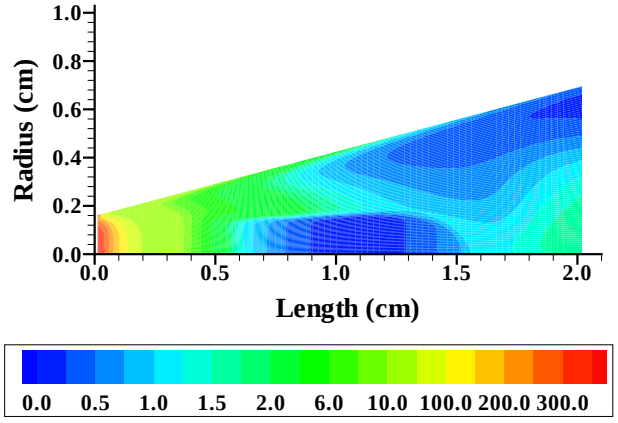

Fig. 9 Energy transfer rate between electrons and heavy particles inside the supersonic diverging nozzle section (in kW/cm^3).

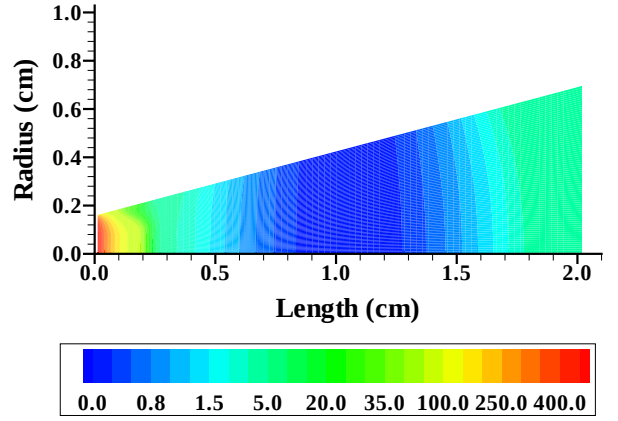

Fig. 10 Joule heating rate of electrons inside the supersonic diverging nozzle section (in kW/cm^3).

stage, this time without energy addition, starting from fixed conditions at the throat, as specified in the flowfield configuration section. As mentioned previously these conditions correspond to the absorption of 5.5 kW of power by the plasma in Stage 1. Without supersonic energy addition the thrust of this hypothetical two-stage thruster is 1.25 N, for 200 mg/sec mass flow rate, and the specific impulse is 640 sec. The results of this calculation show that of the power absorbed in Stage 1, 958 W is transferred to the wall in the supersonic nozzle section due to thermal conduc-

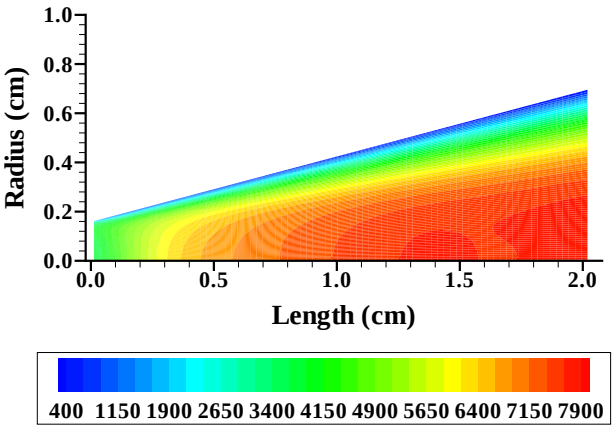

Fig. 11 Axial velocity contours inside the supersonic diverging nozzle section (in m/sec).

tion of the heavy particles. As before, the wall temperature was fixed at 500 K in this calculation. Turning our attention once more to the case of supersonic energy addition we see that when 5 kW of power is added in the supersonic nozzle section, the thrust increases from 1.25 N to 1.49 N and the specific impulse increases from 640 sec to 744 sec. In both respects this corresponds to a 16 % increase. In the case of supersonic energy addition, that amount of power transferred to the wall by thermal conduction also increases from 958 W to 1812 W. These results are summarized in Table 1.

Table 1 Thruster performance without supersonic energy addition, 1, and with supersonic energy addition, 2.

	Power (kW)	Thurst (N)	I_{sp} (sec)	Heat Loss (kW)
1	5.5	1.25	640	0.958
2	10.5	1.49	744	1.812

Conclusions

A fully coupled calculation, solving both the Navier-Stokes and Maxwell equations has been performed for the supersonic energy addition section of the two-stage microwave thruster. A case has been considered for helium propellant where 5.5 kW is deposited in the plenum and an addition 5 kW is absorbed in the supersonic stage, Stage 2. Unlike the previous results with a su-

personic argon flow, where a single-temperature equilibrium model was used and a toroidal plasma formed with most of the energy addition occurring in the subsonic boundary layer, in this work a plasma forms on the centerline, just downstream of the throat. The heat transfer to the wall is markedly reduced, compared to the argon plasma, with only 17 % of the power absorbed in the supersonic section being conducted away to the wall. Another profound difference between the results of this study and those using the single-temperature, equilibrium model, is that the electron number density is more evenly distributed throughout the flow field, as opposed to being sharply concentrated in one location. The question arose as to how much of this was due to the inclusion of non-equilibrium effects in the current model, and how much was influenced by use of helium rather than argon. To answer this question we performed another simulation of the argon flow, using the two-temperature non-equilibrium model, where the mass flow rate was 200 mg/sec, and 660 W was absorbed by the subsonic plasma and 1 kW was absorbed by the supersonic plasma. We conclude that the toroidal plasma formation is a characteristic of the argon flow and not the helium flow. However, although the equilibrium and non-equilibrium models both predict the formation of a toroidal plasma for argon, the non-equilibrium model shows that even with 1 kW supersonic energy addition there is no increase in thrust or specific impulse for this case, with none of the absorbed energy being transferred to the translational motion of the heavy particles. This study highlights the importance of including separate electron temperature and heavy particle temperatures, even at relatively high pressures of several hundred Torr. Any model that describes this kind of microwave heating problem must include a separate electron energy equation.

Now that a fairly complete model, including the effects of separate electron and heavy species temperatures, has been applied to simulate the supersonic stage of the two-stage microwave thruster, several tasks remain in exploring the physics and performance of this thruster. The next step is to do a complete simulation of the entire thruster, both subsonic and supersonic stages, using a more sophisticated numerical grid. This will remove the need to make certain assumptions at the flow conditions at the throat, as discussed in the flowfield configuration section and will allow a detailed study of the stability limit of the subsonic discharge. One would like to operate the thruster so that as much power as possible is absorbed in the subsonic section. Once this limit is determined, a parametric study of energy addition in the supersonic section should be performed, involving cases where the supersonic power is increased further, and where the nozzle geometry and the microwave frequency are varied. The results of this paper show that the specific impulse can be increased by 16 % through the addition of a supersonic stage to the conventional microwave thruster. The model presented here can be a foundation for future parametric studies that can answer the important question of what the performance of a two-stage microwave thruster can ultimately be.

References

[1]R.G. Jahn. *Physics of Electric Propulsion*. McGraw-Hill, 1968.

[2]P. G. Lichon and J. M. Sankovic. Development and demonstartion of a 600-sec mission-average i_{sp} arcjet. *Journal of Propulsion and Power*, 12:1018–1025, 1996.

[3]Y. P. Raizer. *Gas Discharge Physics*. Springer-Verlag, 1997.

[4]S. Whitehair and J. Asmussen. Microwave electrothermal thruster performance in helium gas. *Journal of Propulsion and Power*, 3:136–144, 1985.

[5]D. J. Sullivan and M. M. Micci. Development of a microwave resonant cavity electrothermal thruster prototype. In 23^{rd} *International Electric Propulsion Conference*, Seattle, WA, September 1993. IEPC-93-036.

[6]P. Balaam and M. M. Micci. Investigation of stabilized resonant cavity microwave plasmas for propulsion. *Journal of Propulsion and Power*, 11:1021–1027, 1995.

[7]S. Venkateswaran and C. L. Merkle. Numerical investigation of bluff-body stabilized microwave plasams. *Journal of Propulsion and Power*, 11:357–364, 1995.

[8]D.A. Schwer, S. Venkateswaran, and C. L. Merkle. Analysis of microwave-heated rocket engines for space propulsion. In *AIAA* 29^{th} *Joint Propulsion Conference*, Monterey, CA, June 1993. AIAA 93-2105.

[9]V. P. Chiravalle, R. B. Miles, and E. Y. Choueiri. Numerical simulation of microwave-sustained supersonic plasmas for application to space propulsion. In 39^{rd} *AIAA Aerospace Sciences Meeting*, Reno, NV, January 2001. AIAA-2001-0962.

[10]S. A. Miller and M. Martinez-Sanchez. Two-fluid nonequilibrium simulation of hydrogen arcjet thrusters. *Journal of Propulsion and Power*, 12:112–119, 1996.

[11]T. W. Megli, H. Krier, R. L. Burton, and A. Mertogul. Two-temperature plasma modeling of nitrogen/hydrogen arcjets. *Journal of Propulsion and Power*, 12:1062–1069, 1996.

[12]J. Heiermann and M. Auweter-Kurtz. Numerical and experimental investigation of the current distribution in self-field mpd thrusters. In 37^{rd} *AIAA Joint Propulsion Conference*, Salt Lake City, UT, July 2001. AIAA-2001-3498.

[13]K. Sankaran, S. C. Jardin, and E. Y. Choueiri. Application of a new numerical solver to the simulation of mpd flows. In 36^{rd} *AIAA Joint Propulsion Conference*, Huntsville, AL, July 2000. AIAA-2000-3537.

[14]R. Broglia, M. Manna, H. Deconinck, and G. Degrez. Development and validation of an axisymmetric navier-stokes solver for hypersonic flows. Technical Note 188, von Karman Institute for Fluid Dynamics, 1995.

[15]L. Martinelli. *Calculations of Viscous Flows with a Multigrid Method*. PhD thesis, Princeton University, 1987.

[16]G.L. Brown, A.P. Ratta, R.W. Anderson, L. Martinelli, W.R. Lempert, and R.B. Miles. Fluid mechanics in a radiatively driven hypseronic wind-tunnel - prediction and preliminary experiment. In 19^{rd} *AIAA Advanced Measurement and Ground Testing Technology Conference*, New Orleans, LA, June 1996. AIAA-96-2199.

[17]M. Mitchner and C. H. Kruger. *Partially Ionized Gases*. John Wiley & Sons, 1973.

[18]F. M. White. *Viscous Fluid Flow*. McGraw-Hill, 1974.

[19]S. Ramo, J.R. Whinnery, and T. Van Duzer. *Fields and Waves in Communications Electronics*. John Wiley & Sons, 1965.